https://doi.org/10.1016/j.apenergy.2019.03.072

Flow and heat transfer characteristics of natural convection in vertical air channels of double-skin solar façades*

Tiantian Zhang, Hongxing Yang*

Renewable Energy Research Group (RERG), Department of Building Services Engineering, The Hong Kong Polytechnic University, Hong Kong, China

* Corresponding author: hong-xing.yang@polyu.edu.hk

Abstract: Design and construction of internal ventilated air layers have become a popular way to improve the thermal performance of exterior envelopes in modern buildings. These air layers provide multiple benefits to the building envelopes, including improving the thermal insulation property, as well as achieving the effects of fresh air preheating, space heating, natural ventilation, passive cooling, etc. Obviously, the flow and heat transfer condition of the solar driven natural convection in these air layers can significantly influence the performances of these envelopes. This study numerically investigates the flow and heat transfer process, as well as the influence factors of the temperature and velocity fields, the induced air flowrate and the temperature increase in these air layer structures. The results demonstrate that the flow transition, velocity promotion and temperature increase mainly occur in the near-wall regions. For vertical air layers with the height of 2-4m, the width of 0.1-0.8m, and the input heat flux of 100-400W/m^2, the air flowrate varies between 0.042 kg/s and 0.255kg/s, and the range of the temperature rise is 0.66-14.70℃. For air layers intending to improve ventilation capacity, the channel width should not be bigger than 0.6m, while for those with the purpose of supplying warm air, the width should be lower than 0.2m.

Keywords: Vertical air channel; flow and heat transfer characteristics; natural convection; induced air flowrate; temperature rise

*The short version of the paper was presented at CUE2018, Jun 5-7, Shanghai, China. This paper is a substantial extension of the short version of the conference paper.

Nomenclature		Greek symbols	
c_p	specific heat capacity of air (J/kg℃)	β	thermal expansion coefficient of air
g	gravitational acceleration (m/s^2)	α	thermal diffusivity (m^2/s)
G_k, G_b	rate of turbulent kinetic energy and buoyancy force respectively	ρ	density (kg/m^3)
k	kinetic energy of turbulence (m^2/s^2)	ε	dissipation rate of turbulent kinetic energy (m^2/s^2)
H	air channel height (m)	δ	air channel width (m)
p	pressure (N/m^2)	λ	thermal conductivity (Wm^{-1} K^{-1})
Pr	Prandtl number	μ	dynamic viscosity coefficient (Pa·s)
q_h, q_c	heat flux of the plate (W/m^2)	μ_t	turbulent molecular viscosity
T	temperature (℃)	σ_t	constant of turbulent Prandtl number
u, v	velocity components in the x and y directions respectively (m/s)	σ_k, σ_ε	turbulent Prandtl numbers for k and ε respectively
x, y	Cartesian coordinates (m)	C_μ	turbulent viscosity (Pa·s)
$C_{1\varepsilon}$,$C_{2\varepsilon}$,$C_{3\varepsilon}$	model constants	δ_{ij}	Kronecker delta

1. Introduction

In buildings, exterior envelopes act as the thermal interfaces between the indoor and outdoor environments, thus can greatly influence the indoor thermal condition and the overall energy consumption of indoor air-conditioning systems [1]. As reported, approximately 20%-50% of indoor heating, ventilation and air-conditioning (HVAC) energy consumption is resulted from the heat gain or loss through building envelopes [2]. Actually, the building energy demand is closely linked to exterior envelopes' thermal performances. If the thermal property of a building's envelope is poor and unreasonably designed, excessive heat gain and heat loss will occur in these structures, resulting in a significant increase in the energy requirement of indoor air-conditioning systems. Therefore, it is essential to develop high-performance exterior envelopes to guarantee both low energy consumption and high indoor thermal comfort level for modern buildings.

A number of measures can be taken to enhance building envelopes' thermal performance, such as employing advanced building materials, adding insulation layers, improving the envelope structure [3], etc. Currently, the former two measures have been intensively studied by many researchers, and have become commonly applied in modern building construction. For the third measure, in recent years, a commonly used structural design strategy is to add internal ventilated air layers to building envelopes. Nowadays, various types of air layer involved envelope components can be found in existing buildings, such as Trombe walls [4,5],

solar wall/chimney [6], double-skin façades [7,8], ventilated PV façades [9,10], etc. Air layers used in these components provide multiple benefits for buildings. When the air layer operates in a closed mode, it performs as an extra insulation layer for exterior envelopes, thus improving the thermal insulation property. When the air layer works in an open-ended mode, ventilation channels are generally formed in between the double-layer envelope structures. With the promotion of the buoyancy force resulted from the solar radiation, the ambient air is induced into the channel from the bottom and discharged at the top. The upper and lower vents of the channel could be connected to either the outdoor or the indoor environment, to produce various air circulation patterns. In accordance with the air circulation pattern, multiple functions could be achieved, such as fresh air preheating and supplying, space heating, natural ventilating, and passive cooling [10], as illustrated in Fig.1.

There are numerous literatures focusing on the performances of the air layer envelopes in buildings. Through an experimental study, Chen [11] concluded the effect of using a Trombe wall on reducing the energy demand of an office room. The results indicated that energy saving was 30% when using the Trombe wall. Sun et al. [12] tested and simulated the operating conditions of a PV-Trombe wall with different design configurations. The results verified that employing a window on the south façade was beneficial for indoor warming, but it reduced the thermal efficiency of the wall system by nearly 27%. Hu et al. [13] reported the comparative assessment results of different PV-Trombe walls focusing on the heating/cooling load reduction effect and electricity generation. Hirunlabh et al. [14] investigated the overall performance of a solar chimney made mainly from metallic materials. During their test, when the chimney area was $2m^2$, the induced flowrate achieved 0.01–0.02kg/s, and the indoor heat gain was significantly reduced. Peng et al. [15] evaluated the overall performance of ventilated PV façade under different ventilation strategies. The tested results showed that the ventilated mode performed better for improving the electricity output and reducing the solar heat gain. Yang et al. [16] concluded that the cooling load reduction potential of the ventilated PV wall was 33%-50%. Gagliano et al. [17] studied the thermo-fluid dynamic behavior of an opaque ventilated façade. The numerical results indicated that this façade offered an energy saving potential of 47%-51% depending on climate conditions. Harris [18] comparatively studied the performance of a solar chimney with different inclination angle and surface emissivity through numerical simulations. The results showed that the optimal inclination angle of the solar chimney was 67.5°, with which the energy efficiency was 11% higher than the vertical configuration. Li [19] tested the effect of employing phase change material (PCM) on a solar chimney's performance. The experiment showed that the PCM-combined solar chimney had an acceptable performance, but the performance was greatly influenced by the property of the

PCM. Zamora and Kaiser [20] investigated the performance of a solar chimney driven by the combination of the wind and the buoyancy. A correlation of the non-dimensional mass flowrate was established for this type of solar chimney. Arce et al. [21] experimentally tested the thermal and ventilation behavior of a solar chimney. The results presented that the air temperature promotion through the chimney could reach up to 7.0℃, and the induced air flowrate varied in the region of 50–374m^3/h. Yu et al. [22, 23] evaluated the overall performance of a thermal catalytic Trombe wall. The results verified that this wall system enjoyed an overall energy saving potential o 97.4kWh/m^2, including 64.3kWh/m^2 for space heating and 33.1kWh/m^2 for formaldehyde degradation.

As verified by the aforementioned literatures, using air layers in exterior building envelopes greatly improves the thermal performance, and provides an energy saving potential in indoor air-conditioning. It is noteworthy that the thermal performances and the overall energy efficiencies of these envelopes are closely related to the air flowrate and the air temperature rise through the air channels. Moreover, these two parameters are mainly determined by the flow and heat transfer condition within the internal confined space of the air channels. Therefore, it is essential to identify the operating characteristics of these air channels, as well as to investigate the influence factors of the induced air flowrate and the air temperature rise. Previous research indicated that the airflow and heat transfer processes of the natural convection in the vertical air channels might be laminar or turbulent depending on the channel's thermal condition and geometrical size. As reported, for the vertical air channels in building envelopes, the buoyancy driven natural convection always transforms from the laminar state to the turbulent state as the heat transfer progresses [24]. Although a large number of literatures can be found focusing on the performance of air layer envelopes. However, only a few investigations were reported on the detailed flow and heat transfer process in the vertical air channels.

Some relevant experimental test results were reported. Miyamoto et al. [25] performed a famous experimental study on the heat flux driving natural convection in such vertical air channels, and concluded a correlation equation for the heat transfer for this channel. Fraser et al. [26] reported their test results on the temperature profiles of the air in these vertical channels. La Pica et al. [27] reported their results of the correlations of average Nusselt number and Reynolds number in vertical air channels. Yilmaz and Fraser [24] also reported their tested and simulated results on the profiles of the air velocity and air temperature at different heights of the channel. These investigations provided limited results for the natural convection in the vertical air channels, due to the limitations of the instrumentation and test point arrangement. As a result, numerical methods were employed for detailed study on the operating conditions of these air channels. Fedorov and Viskanta [28]

numerically simulated the temperature and velocity distributions within a vertical channel symmetrically heated by constant heat flux of 80-208W/m^2. Employing the Low Reynolds number k–ε model, the distributions of the Nusselt number and the local heat flux were reported. Reference [29] and [30] reported the simulation results on the convection in the vertical air channels with different thermo-physical conditions and geometrical parameters. Ben-Mansour et al. [31] compared the accuracy of the available turbulent models in predicting the natural convection behavior in vertical air channels. The results presented that the predicted temperature results based on the low Reynolds number k–ε model agreed best with the test results reported in [25], but the differences between the simulation results of standard, renormalization group (RNG), realizable and low Reynolds number k–ε models were very small and could be ignored. Alzwayi and Paul [32] simulated the flow transition phenomenon in the natural convection in vertical air channels. They concluded that the differences between the simulated results from different turbulent models were very small. Gan [33] also compared the suitability of several turbulent models in predicting the flow and heat transfer pattern in vertical air channels. The results showed that the employed models gave similar results for the temperature and velocity field, but the standard k–ε model was more efficient and less time-consuming in the simulation.

Seen from the above analysis, many researchers investigated the natural convection in the vertical air channels of building envelopes, focusing on the air temperature and velocity distributions, and many scholars carried out vast investigations on the performances of different types of air channel involved building envelopes. However, none of these researches aimed at finding the general characteristics of the solar driven natural convection in these air channels. The detailed flow and heat transfer process and its influence factors, the induced air flowrate and the temperature rise through the air channel involved envelopes, have not yet been deeply discussed. Moreover, the relationship between the flow, heat transfer condition and the performances of these envelope components are still not clearly identified. Therefore, there is still a need to perform in-depth study on the flow and heat transfer characteristics in the vertical channels of building envelopes.

This paper aims to present a detailed numerical simulation on the heat flux driving natural convection in the vertical air channels, to investigate the distributions of the air temperature and air velocity. Furthermore, the influences of geometrical sizes and input heat flux on the flowrate and temperature rise through vertical air channels are also necessary to be discussed. The research outcomes can provide necessary technical support for the design and construction of the vertical air channels in building envelopes.

2. Model development

2.1 Physical and mathematical models

All the air channel involved building envelopes have the similar structure. Firstly, these envelopes usually have two structural layers, and an air channel is reserved in between the two structural layers. Secondly, solar absorbing materials, such as solar collector, PV module, absorptive glass, metallic plate, etc., are usually employed in one of the structural layer to absorb as much solar energy as possible. This work focuses on the internal vertical air layer of double-skin solar façades, such as wall solar chimney, Trombe wall, double-skin façades, ventilated PV façades, etc. In these envelope systems, solar radiation activates different air circulation patterns in the vertical air channel, to realize different functions in the building envelope. A simplified two-dimensional physical model of the air channel is established in this paper, as illustrated in Fig.2.

The length of the air channel is H, and the width of the air channel is δ. The left and right sides of the channel are heated by constant heat flux q_c and q_h respectively. The flow in this channel is a natural convection driven by buoyancy. The whole process is assumed as steady state. The physical parameters of the air are assumed constant, except that the density satisfies the boussinesq approximation.

For this natural convection in the vertical channel, a numerical model is established. The governing equations include the conservation equations of mass, momentum and energy, which can be expressed as:

$$\frac{\partial u}{\partial x}+\frac{\partial v}{\partial y}=0 \tag{1}$$

$$\rho u\frac{\partial u}{\partial x}+\rho v\frac{\partial u}{\partial y}=-\frac{\partial p}{\partial x}+\frac{\partial}{\partial x}\left[\left(\mu+\mu_t\right)\frac{\partial u}{\partial x}\right]+\frac{\partial}{\partial y}\left[\left(\mu+\mu_t\right)\frac{\partial u}{\partial y}\right] \tag{2}$$

$$\rho u\frac{\partial v}{\partial x}+\rho v\frac{\partial v}{\partial y}=-\frac{\partial p}{\partial y}+\frac{\partial}{\partial x}\left[\left(\mu+\mu_t\right)\frac{\partial v}{\partial x}\right]+\frac{\partial}{\partial y}\left[\left(\mu+\mu_t\right)\frac{\partial v}{\partial y}\right]+\left(\rho-\rho_0\right)g \tag{3}$$

$$\rho u\frac{\partial T}{\partial x}+\rho v\frac{\partial T}{\partial y}=\frac{\partial}{\partial x}\left[\left(\frac{\lambda}{c_p}+\frac{\mu_t}{\mathrm{Pr}_t}\right)\frac{\partial T}{\partial x}\right]+\frac{\partial}{\partial y}\left[\left(\frac{\lambda}{c_p}+\frac{\mu_t}{\mathrm{Pr}_t}\right)\frac{\partial T}{\partial y}\right] \tag{4}$$

In laminar regime, the above equations are solved directly, as the turbulent viscosity μ_t is zero due to the flow pattern. In turbulent regime, the turbulent viscosity should be determined by turbulent models. The standard k-ε model is employed, which can be defined as:

$$\rho u\frac{\partial k}{\partial x}+\rho v\frac{\partial k}{\partial y}=\frac{\partial}{\partial x}\left[\left(\mu+\frac{\mu_t}{\sigma_k}\right)\frac{\partial k}{\partial x}\right]+\frac{\partial}{\partial y}\left[\left(\mu+\frac{\mu_t}{\sigma_k}\right)\frac{\partial k}{\partial y}\right] + G_k+G_b-\rho\varepsilon \tag{5}$$

$$\rho u\frac{\partial \varepsilon}{\partial x}+\rho v\frac{\partial \varepsilon}{\partial y}=\frac{\partial}{\partial x}\left[\left(\mu+\frac{\mu_t}{\sigma_\varepsilon}\right)\frac{\partial \varepsilon}{\partial x}\right]+\frac{\partial}{\partial y}\left[\left(\mu+\frac{\mu_t}{\sigma_\varepsilon}\right)\frac{\partial \varepsilon}{\partial y}\right] + C_{\varepsilon 1}\frac{\varepsilon}{k}\left(G_k+C_{\varepsilon 3}G_b\right)-C_{\varepsilon 2}\rho\frac{\varepsilon^2}{k} \tag{6}$$

In the above equations, Pr_t, σ_k, σ_ε are Prandtl numbers for T, k, and ε, the values are 0.9, 1.0 and 1.3 respectively [34]. G_k is the generation rate of kinetic energy; G_b is the buoyancy force; μ_t represents the turbulent viscosity; δ_{ij} is the Kronecker delta; C_u, $C_{1\varepsilon}$, $C_{2\varepsilon}$, $C_{3\varepsilon}$ are constants with the values of 0.09, 1.44, 1.92 and 1.0 respectively [35]. G_k ,G_b , μ_t and δ_{ij} can be determined as:

$$G_k=\mu_t\left(\frac{\partial u_i}{\partial x_j}+\frac{\partial u_j}{\partial x_i}\right)\frac{\partial u_i}{\partial x_j}-\frac{2}{3}\rho k\delta_{ij}\frac{\partial u_i}{\partial x_j} \tag{7}$$

$$G_b=\beta g_i\frac{\mu_t}{Pr_t}\frac{\partial T}{\partial x_i};\ \mu_t=\rho C_\mu\frac{k^2}{\varepsilon};\ \delta_{ij}=\begin{cases}0 & if\ i\neq j\\ 1 & if\ i=j\end{cases} \tag{8}$$

At the inlet of the vertical air channel, the boundary pressure and temperature conditions of the air are set according to the real ambient environment. On both of the sides, uniform heat fluxes are imposed on both sides of the channel. The turbulent kinetic energy and the dissipation energy are set as zero at the sides. At the outlet, ambient pressure is applied and the temperature gradient is set to be zero.

The boundary conditions can be expressed as:

$$\begin{cases} x=0, q=q_c, u=0, v=0, k=0;\\ x=\delta, q=q_h, u=0, v=0, k=0;\\ y=0,\ p=p_0, T=T_0, k=0, \varepsilon=0;\\ y=H,\ p=p_0, \dfrac{\partial T}{\partial y}=0. \end{cases} \tag{9}$$

For the thermal boundary conditions at the left and right sidewalls of a vertical channel envelope, there is a fixed ratio between q_c and q_h. Fig.3 illustrates the typical energy flows in these envelopes. When sun light arrives at the exterior glazing, most of the solar radiation passes through, and a small portion is reflected and absorbed by the glazing; furthermore, most of the transmitted solar radiation is absorbed by the absorber, and a small part is reflected; when the reflected part re-passes the exterior glazing, transmission, absorption and reflection effects occur again. Therefore, heat fluxes are imposed on both sides of the vertical air channel.

When the transmission, reflection and absorption coefficients of the glazing and the absorber are determined, a fixed correlation can be found between these two fluxes. For this study, assume the transmission, reflection and absorption coefficients of the glazing are 0.85, 0.09 and 0.06, and the transmission and reflection coefficients of the absorber plate is 0.95 and 0.05 respectively. The ratio between the heat fluxes on the glazing side and the absorber side is 0.077 (q_c/q_h=0.077). This proportion will be uses in the boundary conditions of the simulation work of this study.

Using the established model, the temperature and velocity fields of the air in the channel can be predicted; consequently, the natural convection characteristics can be analyzed and summarized.

2.2 Grid independence test and model validation

The finite volume method is employed to discretize the governing equations, and the second-order upwind scheme is adopted to solve the discrete equations. The SIMPLE algorithm is employed to couple the velocity and pressure during the solution. Enhanced wall function is employed to cope with the large gradients in temperature and velocity in the near-wall regions. All the discretization and solution are performed in the Fluent 6.3 software.

A grid independence test was conducted before the case studies to find out the suitable grid size for solving the flow and heat transfer problems in vertical air channels. For the channel with the size of 400mm×3000mm, the test was performed by employing mesh sizes of 40×100, 60×150, 80×180, 120×200, 160×300, and 200×400. Non-uniform structured meshes were made with clustering near the inlet, outlet and sidewall regions. When the heat flux of 200W/m^2 was imposed on the right wall, the results show that the grids of 40×100, 60×150, and 80×180 overestimated the turbulent kinetic energy of the flow. The grids of 120×200, 160×300, and 200×400 gave results that were more satisfactory. The differences among the results were almost negligible. Therefore, all these three grids were applicable for this problem. To save computational time, the grid of 120×200 was the most suitable mesh scheme. Furthermore, for the channels with other sizes, similar mesh scheme can be employed.

To evaluate the model reliability and accuracy, the simulation results obtained from the established model were compared to the experimental results reported in reference [24]. The simulation was performed in accordance with the experimental condition in [24], in which the inlet temperature was 23℃, the inlet turbulent intensity was measured as 13%, and the right wall temperature was kept to be 100℃. Fig.4 presents the comparisons between the numerical and experimental results of the turbulent kinetic energy, the velocity and temperature, respectively. For the

turbulent kinetic energy profiles illustrated in Fig.4(a), although observable difference can be found between the numerical and experimental results, the changing tendencies are similar at the given heights of the channel. So the established model can provide satisfactory turbulent kinetic energy prediction. As demonstrated in Fig.4(b), the velocity profiles of the numerical results at the channel heights of 0.09m, 1.50m and 2.97m show very good agreements with the experimental results. It can be also found that the established model gave a close predicted results of the temperature field, when compared with the test results, as shown in Fig.4(c).

To sum up, the established numerical model and the solution techniques can provide satisfactory prediction results for the temperatures and velocities in the vertical channel, and can show properly the variation tendencies of the turbulent kinetic energy. Therefore, the established model can be used to perform the numerical simulations for the natural convection of the vertical air channel in the following sections.

3. Flow and heat transfer characteristics of the heat flux driving natural convection in the vertical channel

In this study, numerical simulations were performed on the vertical air channels with different geometrical sizes and heat fluxes. The channel width ranges from 0.1m to 0.8m and the height changes between 2m and 4m. The input heat fluxes on the right wall ranges from 100W/m^2 to 400W/m^2; accordingly, as mentioned above, the input heat fluxes on the left wall ranges from 7.7W/m^2 to 30.8W/m^2. The inlet temperature is set to be 20℃.

3.1 The evolution of the flow and heat transfer in the channel

To investigate the internal flow transition process in vertical channels, Fig.5 illustrates the distributions of the turbulent kinetic energy in the channels with different widths, when the channel height is 3m and the heat flux is 200W/m^2.

As the figure shows, the turbulent kinetic energy increases along the sidewall due to the input heat flux. A complicated distribution is presented when the width is 0.1m. When the width is larger than 0.2m, the kinetic energy increases along the sidewall and reaches the maximum at the top. The values near the sidewalls are clearly higher than in other regions, since the input heat flux is the driving force of the whole process. The changing tendencies of the turbulent kinetic energy show that the airflow in the channel translates from laminar to turbulent in the near-wall regions of the sidewalls.

Fig.6 illustrates the velocity fields of the air channels with different widths. The

velocities near the sidewalls are much higher than in the central region. Along the sidewalls, the velocity keeps increasing with the height increase, and at the outlet, the maximal velocity would reach around 0.85m/s for all the vertical channels with the width from 0.1m to 0.8m. In the central region, the velocity gradually decreases when the height increases. The minimum velocity points locate at the center of the exit. Moreover, the exit velocity in the central region declines with the increase of the channel width: the larger the width, the lower the exit velocity is. The velocity fields reveal the fact that the velocity improvement of the internal air mainly occurs in the near-wall regions, while the air velocity gradually decreases in the middle region. Therefore, increasing the channel width can help to improve the flowrate through the channel, but when the width exceeds a limit, the improvement may be unremarkable. Namely that, the flowrate induced by the heat flux will not continue to grow when the channel width exceeds a critical value.

Fig.7 shows the temperature fields of the air channels with different widths. Seen from the temperature contours, the heating effect of the heat flux on the internal air mainly occurs in the adjacent regions of the sidewalls. The maximal temperatures at the exit reach higher than 60℃ for all these channels. Moreover, the larger the width, the higher the peak temperature is. For instance, when the width is 0.2m, the peak temperature at the exit is 62℃; when the width increases to 0.8m, the maximal temperature is improved to 72℃. When the width exceeds 0.3m, at the exit, there is still a large unheated part in the internal area. The larger the width, the bigger the unheated region is.

3.2 Changing tendencies of the turbulent kinetic energy, velocity and temperature along the channel height

To investigate the variation tendencies of the key parameters in the natural convection, Fig.8-10 illustrate the changing curves of turbulent kinetic energy, velocity and temperature at different heights of the channels.

The curves in Fig.8 indicate that the turbulent kinetic energy grows as the flow and heat transfer progresses. In each channel, the peak value occurs at the top and near the right sidewall. The values are higher in the near-wall regions than in the central regions. With constant heat fluxes imposed on the sidewalls of the channel, the induced flow grows more and more chaotic, especially in the near-wall regions of the side walls, thus the flow pattern translates from laminar to turbulent along the sidewalls.

As the velocity curves showed in Fig.9, for the channels with four different widths, in the near-wall regions, the velocity increases with the height increase. The

exit velocities reach approximately 0.90m/s for these channels. In the adjacent region of the left wall, for the channel with 0.2m in width, the velocity decreases as the height increase, while for the other three channels, the velocity increases with the height increase. In the central region of the channel, the velocity gradually decreases. For vertical channels with these four widths, the exit velocities near the left wall and the right wall can reach up to around 0.35m/s and 0.9m/s, respectively, which indicate that when constant heat fluxes are imposed on the sidewalls of the channel, the channel width just poses a weak effect on the exit velocity.

As illustrated in Fig.10, the temperature variation curves at different heights show that the constant input flux at the left and right boundaries can generally improve the air temperature in the vertical channel, and the affected zones vary a lot when the width is different. For the channel with the width of 0.2m, the exit air temperatures in all locations are improved. When the width is larger than 0.4m, only the air in adjacent regions of the sidewall is heated. For the channels with the widths of 0.4m, 0.6m and 0.8m, the unaffected regions are 0.08-0.25m, 0.1m-0.45m and 0.17-0.60m, respectively. Therefore, for solar heated vertical channels, when the channel width is smaller than 0.2m, the input heat flux can affect all the internal region of the channel. When the width is larger, the heating effectiveness is limited in the adjacent regions of the sidewalls. Therefore, the effect of the channel width on the air heating has limitation, since the heating occurs only within a very small area near the sidewalls. If the purpose of employing the air channel is to achieve an optimal air heating effectiveness, the width should not exceed the limitation.

From the above analysis, we can conclude that, the values of the turbulent kinetic energy, the velocity and the temperature in the near-wall regions are much higher than those in the central region. Therefore, for heat flux driven turbulent natural convection in vertical air channels, the flow transition, velocity and temperature increase mainly occur in the near-wall regions, since the input heat flux creates boundary layers of temperature and velocity variations.

4. Influences of geometry parameters and input heat flux on the turbulent kinetic energy, velocity and temperature fields

In the natural convection of a vertical channel, the flow and temperature distributions are influenced by many factors, such as the channel size and the heat flux boundary. In this section, the effect of these factors will be assessed.

4.1 The effect of channel height

The channel height has a great impact on the evolution of the convection, since it determines the total energy input. Fig.11 demonstrates the turbulent kinetic energy

profiles along the width at the middle (y/H=0.5) and the exit (y/H=1) of the vertical channels with height from 2m to 4m, when the heat flux is 200W/m^2 and the width is 0.4m. As can be viewed, increasing the channel height can generally improve the turbulent kinetic energy values. The heat flux affected regions and the changing tendencies are almost the same under the channel height from 2m to 4m.

Fig.12 presents the velocity profiles along the width at the middle and the exit of the vertical channel. At the middle and exit cross-sections, the velocity generally improves when the channel height increases. The velocity distributions of the channels with different heights are similar. At the middle section, the velocities near the sidewalls are promoted by the heat flux, when compared with those of the center region. At the exit, the velocities near the sidewalls are further improved, while the velocities at the central region are reduced, compared with those at the middle section.

Fig. 13 illustrates the temperature profiles at the middle and the exit of the vertical channel. The results show that the height has a weak influence on the temperature field. At these two sections, the temperatures near the sidewall increases slightly with the increase of the height. Therefore, the height has a big impact on the turbulent kinetic energy and velocity distributions, but has little effect on the temperature field in a vertical channel.

4.2 The effect of channel width

When the height is constant, the channel width determines the extent of the restricting effect of the narrow space on the natural convection. Fig.14 shows the influence of the channel width on turbulent kinetic energy profiles at the middle and exit of the channel. As can be seen, both at the middle and at the exit, when the width is below 0.2m, an increase in the channel width can reduce the peak values near the sidewalls. When the width is larger than 0.3m, an increasing channel width leads to a reduction in the peak value near the left wall and an increase in the peak value near the right wall. Therefore, the channel width has a great influence on the turbulence intensity of the internal flow. Under the same heat flux input and channel height, a bigger channel width can result in a more chaotic natural convection flow in the channel.

Fig.15 shows the velocity profiles at the middle and the exit of the channel. At the middle sections of these channels, the peak values of the velocity occur in near the right wall. When the width is lower than 0.3m, along the horizontal axis, the velocity increases rapidly in the adjacent region of the left wall, grows slowly in the central region, again improves sharply and decreases dramatically in the adjacent region of the right wall. When the width is bigger than 0.4m, the velocity increases first and then decreases a little in the left near-wall region. The peak velocity value

firstly decreases and then stays almost constant with the increase of the channel width, and the turning point of this tendency occurs when the width is 0.3m. The velocities of central regions decrease with the increase of the width. When the channel width increases from 0.2m to 0.8m, the central velocity decreases from 0.48m/s to 0.15m/s, but the decline rate decreases gradually. At the exit, the maximal velocity also occurs near the right wall. For the channels with the width from 0.1m to 0.8m, the values of the peak velocities are all around 0.87m/s. Similar to the velocity-changing tendency of the middle sections, the central region velocity decreases as the width grows. Thus, the channel width has a weak impact on the peak velocity both at the middle and the exit of the channel, but it significantly affects the velocity profile in the central region.

Fig.16 illustrates the temperature profiles. At the middle section, when the width is 0.1m, the temperature values at all locations are higher than 20℃, indicating that the internal air are completely heated due to the given heat flux. But when the width is bigger than 0.2m, only the air in the near-wall regions are warmed, the air temperatures in the central region remain 20℃, namely that the air in this region are unheated. The peak temperature near the right wall increases along as the width, as the width varies from 0.2m to 0.8m, the peak temperature increases from 61.58℃ to 72.20℃. At the exit, the temperature variations are similar to those of the middle sections. The internal air is completely heated when the width is 0.1m and 0.2m; however, when the width is larger than 0.3m, the airs in the central regions remain unheated. The peak temperatures at the exit are around 35℃ for all the channels with the width from 0.1m to 0.8m. The peak temperatures are lower at the exit than at the middle section, but the affected area increases.

4.3 The effect of input heat flux

Fig.17 shows the turbulent kinetic energy profiles along the width at the middle and the exit of the channel with the width of 0.4m and the height of 3m, under different heat fluxes. Similarly, increasing the heat flux can generally improve the turbulent kinetic energy values. The heat flux affected regions and the changing tendencies are almost the same with different heat fluxes.

Fig.18 illustrates the velocity profiles along the width at the middle and the exit of the channel. As the heat flux increases, the air velocity generally improves, both at the middle and at the exit, but the increasing rate gradually declines. Compared with the velocities along the middle section, the velocities along the exit are further improved.

Fig.19 presents the temperature profiles at the middle and the exit of the channel. As the figure indicates, increasing the input heat flux helps to improve the air

temperature in the near-wall regions. When the flux increases from 100W/m^2 to 400W/m^2, in the middle section, the peak temperature near the left wall raises from 24.14℃ to 31.13℃, and the peak temperature near the right wall increases from 47.44℃ to 93.69℃. At the exit, the peak temperature near the left wall raises from 24.32℃ to 30.58℃, and the peak temperature near the right wall increases from 44.22℃ to 83.67℃. The increasing rate of the peak temperature declines as the flux increases. The peak temperatures of the exit are lower than that in the middle section, while the affected region enlarges.

Through the above discussions on the influence factors, the influence of the channel height and input heat flux are similar, since these two parameters determine the energy input in this flow and heat transfer process in vertical channels. Increases in channel height and heat flux can generally improve the values of turbulent kinetic energy and velocity, but the size of the heat flux affected region and the temperature profiles are weakly influenced by these two factors. The channel width greatly influences the internal temperature, velocity and turbulent kinetic energy field, as it determines the extent of the restricting effect of the narrow space on the natural convection.

5. Influence factors of temperature rise and induced flowrate

Due to the purpose of using air channels in building envelopes, the airflow rate and air temperature rise across the vertical channel are worthy of investigating. The simulation results show that for vertical channels with the height of 2-4m, the width of 0.1-0.8m, and the input heat flux of 100-400W/m^2, the air flowrate varies between 0.042 kg/s and 0.255kg/s, and range of the temperature rise is 0.66-14.70℃.

Fig.20 illustrates the changing tendencies of the flowrate and temperature rise with the channel height under different heat flux conditions, when the width is 0.4m. The curves show that, when the heat flux and the channel width are constant, the increase in the height can result in a rapid improvement in the flowrate and the temperature. The larger the heat flux input, the bigger the growth rates will be produced by the height increase, both for the flowrate and the temperature rise. When the heat flux is 100W/m^2, 200W/m^2, 300W/m^2 and 400 W/m^2, the growth rates of the flowrate are 0.036, 0.045, 0.051 and 0.057kg/(m·s), and the growth rates of the temperature rise are 0.245, 0.391, 0.517 and 0.628 K/m, respectively. The reason may be that, the larger the channel height, the longer the retention time of the air, and the better the heating effectiveness could be achieved.

Fig.21 illustrates the changing tendencies of the flowrate and temperature rise with the channel width under different heat flux conditions, when the height is 3m. As the figure indicates, the air flowrate improves with the increase of the width, but

the growth rate becomes lower and lower. Therefore, when the channel height is constant, if the width grows to a certain value, the influence of the width on the flowrate is weak. Taking the heat flux of 100 W/m^2 for instance, when the height is 3m, as the width grows from 0.1m to 0.6m, the flowrate increases from 0.056kg/s to 0.121kg/s. However, when the width further grows to 0.8m, the flowrate only improves to 0.124kg/s. Therefore, when the channel width is lower than 0.6m, the effect of the width on the flowrate is quite significant, but when the width is bigger than 0.6m, the flowrate only increase slightly with the width increase. Accordingly, for the vertical channel with the purpose of promoting ventilation effect, the width should be lower than 0.6m.

Similarly, the temperature rise decreases with the width increase, but the reduction rate gradually declines. When the width exceeds a critical value, the temperature rise caused by width increase will be very limited and can be ignored. Thus, for the channels with the purpose of hot air supplying, the width should not be too big. For instance, when the heat flux is $300W/m^2$ and the width is 0.2m, the temperature rise is below 6℃. Considering the return air temperature of a room, the temperature rise may not be sufficient to satisfy the requirement of the supply air temperature. Thus, for this purpose, the channel width should be lower than 0.2m.

Fig.22 presents the changing tendencies of the flowrate and temperature rise with the heat flux under different widths, when the height is 3m. As the figure shows, the air flowrate improves with the increase of the heat flux, but the growth rate gradually decreases when the width increases. When the heat flux increases from $50W/m^2$ to $400W/m^2$, for the channel with the height of 3m and the width of 0.1m, the flowrate grows from 0.047kg/s to 0.092kg/s. Therefore, the effect of the heat flux is considerable.

The temperature rise also increases with the heat flux increase, but the growth rate gradually decreases. The smaller the channel width, the greater the effect of the heat flux on the temperature rise is. When the width is bigger than 0.2m, the heating effect on the airflow is weak, thus the temperature rise is low. As a result, the heating capacity of the warmed air is poor. Taking the channel with the width of 0.3m as an example, when the heat flux is $400W/m^2$, the temperature rise is only 4.41℃.

For the heat flux driven natural convection in vertical channels, the channel height and the input heat flux can significantly affect the induced air flowrate and the average temperature rise. Increases in these two parameters may result in a straight increase in the flowrate and the temperature rise, as the energy input of the flow and heat transfer greatly improves. The channel width has a weak effect on the flowrate and the temperature rise. The flowrate improves, while the temperature decreases with the increase of the width, and the rate of change becomes lower and

lower. When the channel height is constant, if the width exceeds a critical value, the influence of the width on the flowrate and temperature rise becomes negligible. For practical applications of vertical air channels in buildings, the height should be as bigger as possible. For air channels intending to improve ventilation capacity, the channel width should be below 0.6m, while for channels with the purpose of supplying warm air, the width should be lower than 0.2m.

6. Conclusions

This study investigates the flow and heat transfer characteristics of natural convection in vertical air channels of building envelopes. Based on the above results and discussions, the following conclusions have been drawn:

For the heat flux driving natural convection in vertical air channels, the values of the turbulent kinetic energy, the velocity and the temperature in the near-wall regions are much higher than in the central region of the vertical channel. Therefore, the flow transition, velocity and temperature increase mainly occur in the near-wall regions.

The influences of the channel height and input heat flux are similar. Increases in channel height and heat flux can generally increase the values of turbulent kinetic energy and velocity, but the size of the heat flux affected region and the temperature profile are weakly influenced. The channel width greatly influences the internal temperature, velocity and turbulent kinetic energy field, since it determines the extent of the restricting effect of the narrow space on the natural convection.

For vertical channels with the height of 2-4m, the width of 0.1-0.8m, and the input heat flux of 100-400W/m^2, the air flowrate varies between 0.042 kg/s and 0.255kg/s, and range of the temperature rise is 0.66-14.70℃. The influences of channel height and heat flux on induced flowrate and temperature rise are significant, while the influence of channel width is limited. Increases in the channel height and the input heat flux may result in a straight increase in the flowrate and the temperature. The flowrate improves, while the temperature decreases with the increase of the width, but the rate of change becomes lower and lower.

For practical applications of vertical air channels in buildings, there are critical values for the channel width. For air channels intending to improve ventilation capacity, the channel width should not be bigger than 0.6m, while for channels with the purpose of supplying warm air, the width should be lower than 0.2m.

Acknowledgements

This research was supported by The Hong Kong Polytechnic University Postdoctoral Fellowships Scheme (G-YW2E).

References

[1] Fang Z, Li N, Li B, Luo G, Huang Y. The effect of building envelope insulation on cooling energy consumption in summer. Energy & Buildings, 2014, 77(7):197–205.

[2] Yu J, Tian L, Xu X, Wang J. Evaluation on energy and thermal performance for office building envelope in different climate zones of China. Energy & Buildings, 2015, 86:626-639.

[3] Sozer H. Improving energy efficiency through the design of the building envelope. Building & Environment, 2010, 45(12):2581–2593.

[4] Sadineni S B, Madala S, Boehm R F. Passive building energy savings: A review of building envelope components. Renewable & Sustainable Energy Reviews, 2011, 15(8):3617-3631.

[5] Stevanović S. Optimization of passive solar design strategies: A review. Renewable & Sustainable Energy Reviews, 2013, 25:177-196.

[6] Chan H Y, Riffat S B, Zhu J. Review of passive solar heating and cooling technologies. Renewable & Sustainable Energy Reviews, 2010, 14(2):781–789.

[7] Barbosa S, Ip K. Perspectives of double skin façades for naturally ventilated buildings: A review[J]. Renewable & Sustainable Energy Reviews, 2014, 40:1019-1029.

[8] Agathokleous R A, Kalogirou S A. Double skin facades (DSF) and building integrated photovoltaics (BIPV): A review of configurations and heat transfer characteristics[J]. Renewable Energy, 2016, 89:743-756.

[9] Chi-Ming Lai, ShuichiHokoi. Solar façades: A review[J]. Building & Environment, 2015, 91: 152-165.

[10] Zhang T, Tan Y, Yang H, Zhang X. The application of air layers in building envelopes: A review. Applied Energy, 2016,165: 707–734.

[11] Chen B, Chen H J, Meng S R, Chen X, Sun P, Ding Y. The effect of Trombe wall on indoor humid climate in Dalian, China. Renewable Energy, 2006, 31(3):333–343.

[12] Sun W, Ji J, Luo C, He W. Performance of PV-Trombe wall in winter correlated with south façade design. Applied Energy, 2011, 88(1): 224-231

[13] Hu Z, He W, Ji J, Hu D, Lv S, Chen H, Shen Z. Comparative study on the annual performance of three types of building integrated photovoltaic (BIPV) Trombe wall system[J]. Applied Energy, 2017, 194:81-93.

[14] Hirunlabh J, Kongduang W, Namprakai P, Khedari J. Study of natural ventilation of houses by a metallic solar wall under tropical climate. Renewable Energy, 1999, 18(1):109–119.

[15] Peng J, Lu L, Yang H, Ma T. Comparative study of the thermal and power performances of a semi-transparent photovoltaic façade under different ventilation modes. Applied Energy, 2015,138, 572-583.

[16] Yang H, Burnett J, Ji J. Simple approach to cooling load component calculation through PV walls. Energy & Buildings, 2000, 31(3):285-290.

[17] Gagliano A, Nocera F, Aneli S. Thermodynamic analysis of Ventilated Façades under different wind conditions in summer period [J]. Energy & Buildings, 2016, 122:131-139.

[18] Harris D J , Helwig N. Solar chimney and building ventilation[J]. Applied Energy, 2007, 84(2):135-146.

[19] Li Y C , Liu S L . Experimental study on thermal performance of a solar chimney combined with PCM[J]. Applied Energy, 2014, 114(114):172-178.

[20]Zamora B, Kaiser A S. Numerical study on mixed buoyancy-wind driving induced flow in a solar chimney for building ventilation[J]. Renewable Energy, 2010, 35(9):2080-2088.

[21] Arce J, Jiménez M J, Guzmán J D, Heras M R, Alvarez G, Xaman J. Experimental study for natural ventilation on a solar chimney[J].Renewable Energy, 2009, 34(12):2928-2934.

[22] Yu B, He W, Li N, Wang L, Cai J, Chen H, Ji J, Xu G. Experimental and numerical performance analysis of a TC-Trombe wall [J]. Applied Energy, 2017, 206:70-82.

[23] Yu B, Hou J, He W, Liu S, Hu Z, Ji J, Chen H, Xu G. Study on a high-performance photocatalytic-Trombe wall system for space heating and air purification [J]. Applied Energy, 2018, 226:365-380.

[24] T. Yilmaz, S.M. Fraser, Turbulent natural convection in a vertical parallel-plate channel with asymmetric heating, Int. J. Heat Mass Transfer 50 (2007) 2612–2623.

[25] M. Miyamoto, Y. Katoh, J. Kurima, H. Sasaki, Turbulent free convection heat transfer from vertical parallel plates, in: C.I. Tien, V.P. Carey, J.K. Ferrel (Eds.), Heat Transfer, vol. 4, Hemisphere, Washington, DC, 1986, pp. 1593–1598.

[26] S.M. Fraser, A. Gilchrist, T. Yilmaz, Natural convection LDA measurements, in: A. Dybbs, B. Ghorashi (Eds.), Laser Anemometry Advances and Applications, ASME, New York, 1991, pp. 547–554.

[27] A. La Pica, G. Rodono, R. Volpes, An experimental investigation on natural

convection of air in a vertical channel, Int. J. Heat Mass Transfer 36 (1993) 611–616.

[28] A.G. Fedorov, R. Viskanta, Turbulent natural convection heat transfer in an asymmetrically heated, vertical parallel-plate channel, Int. J. Heat Mass Transfer 40 (1997) 3849–3860.

[29] S.A.M. Said, M.A. Habib, H.M. Badr, S. Anwar, Turbulent natural convection between inclined isothermal plates, Comput. Fluids 34 (2005) 1025–1039.

[30] H.M. Badr, M.A. Habib, S. Anwar, Turbulent natural convection in vertical parallel-plate channels, Heat Mass Transfer 43 (2006) 73–84.

[31] R. Ben-Mansour, M.A. Habib, H.M. Badr, S. Anwar, Comparison of different turbulent models and flow boundary conditions in predicting turbulent natural convection in a vertical channel with isoflux plates, Arabian J. Sci. Eng. 23 (2006) 191–218.

[32] A. S. Alzwayi, M. C. Paul, Effect of width and temperature of a vertical parallel plate channel on the transition of the developing thermal boundary layer. International Journal of Heat and Mass Transfer 63 (2013) 20–30.

[33] Gan G. Simulation of buoyancy-induced flow in open cavities for natural ventilation[J]. Energy & Buildings, 2006, 38(5):410-420.

[34] R. Ben-Mansour, M.A. Habib, H.M. Badr, S. Anwar, Comparison of different turbulent models and flow boundary conditions in predicting turbulent natural convection in a vertical channel with isoflux plates, Arabian J. Sci. Eng. 23 (2006) 191–218.

[35] B. Zamora, A.S. Kaiser. Optimum Wall-to-wall Pacing in Solar Chimney Shaped Channels in Natural Convection by Numerical Investigation. Applied Thermal Engineering, 2009, 29(4):762-769.

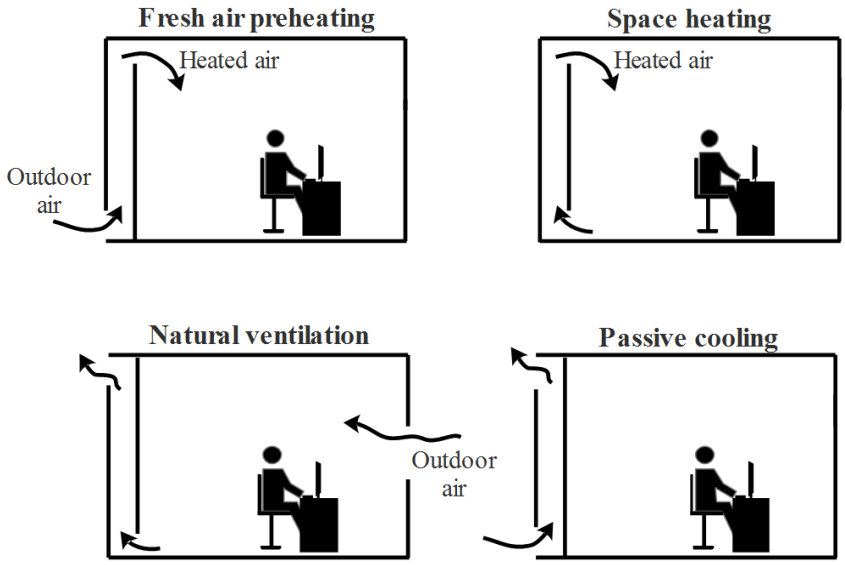

Fig.1 Different operation modes of ventilated air channels

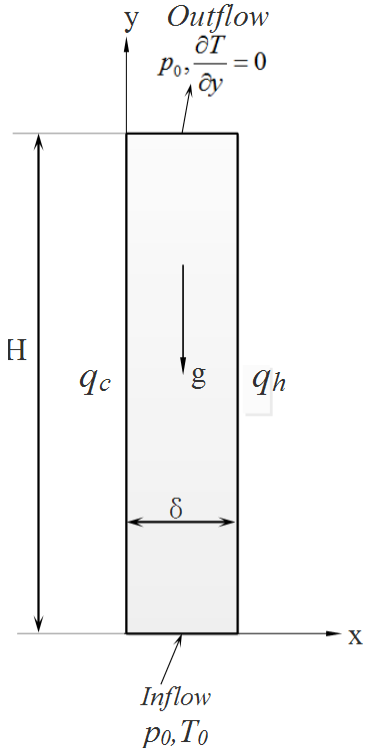

Fig.2 Physical model of airflow and heat transfer in the air channel

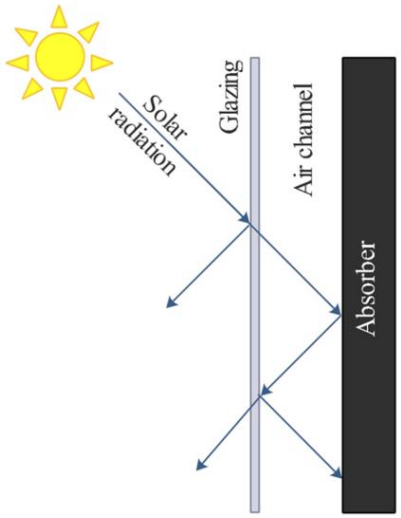

Fig.3 Energy flows in the air channel of double-layer glazed building envelope

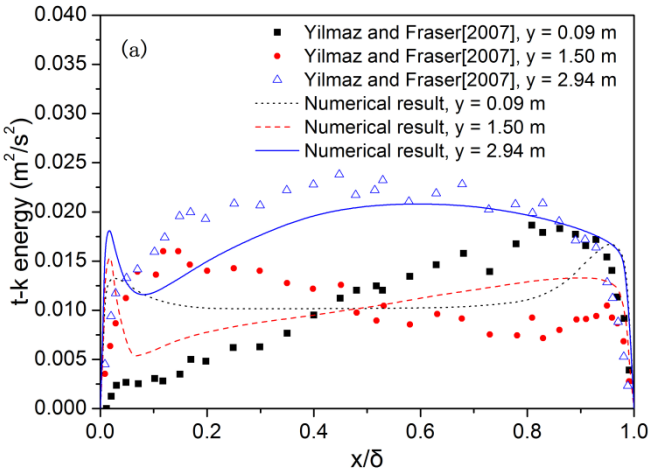

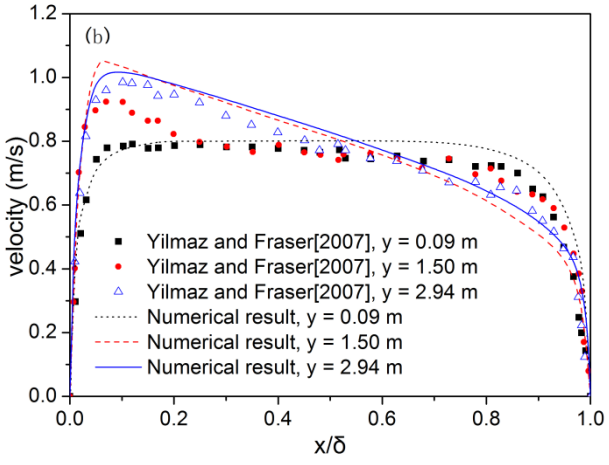

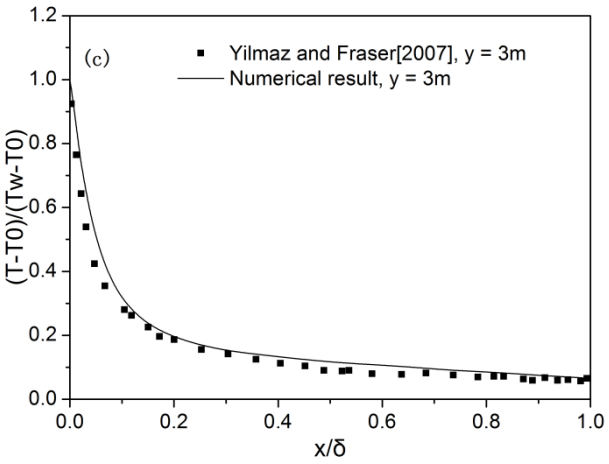

Fig.4 Validation of mathematical model on turbulent kinetic energy (a), velocity (b), and temperature (c) profiles

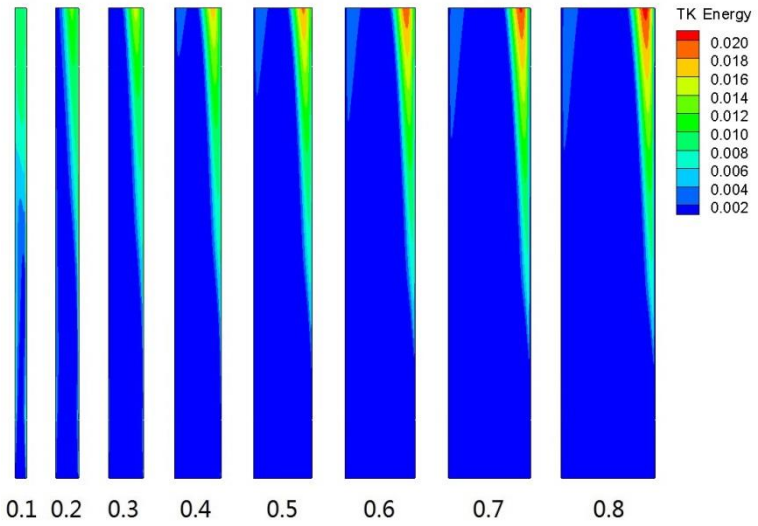

Fig.5 Distribution of the turbulent kinetic energy in vertical channels with different widths (with height of 3m and heat flux of 200W/m^2)

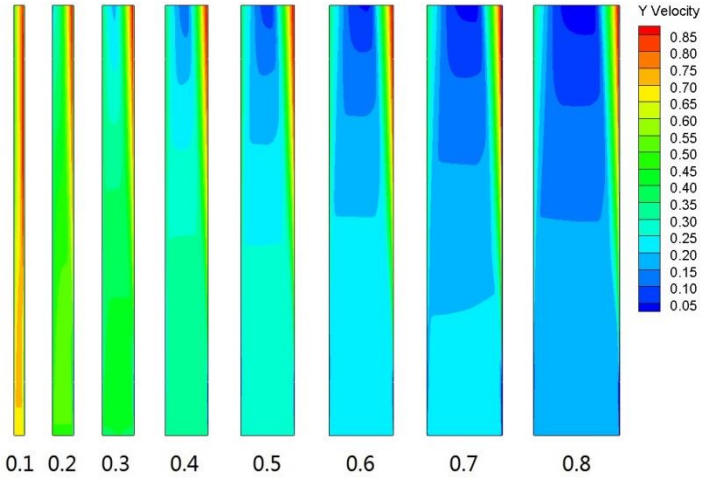

Fig. 6 Distribution of the velocity in vertical channels with different widths (with height of 3m and heat flux of 200W/m^2)

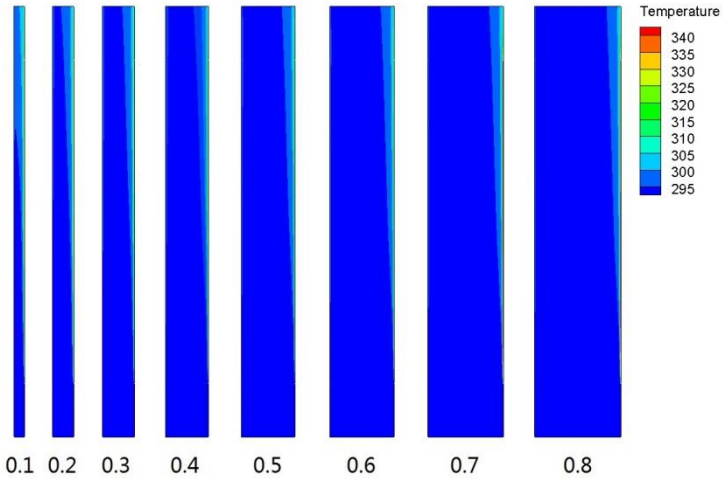

Fig. 7 Distribution of the air temperature in vertical channels with different widths (with height of 3m and heat flux of 200W/m^2)

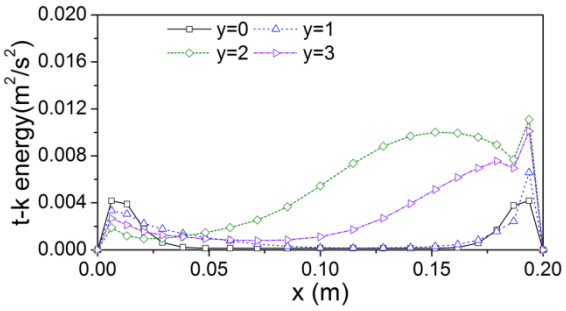

a) H=3m, q_h=200W/m^2, δ=0.2m

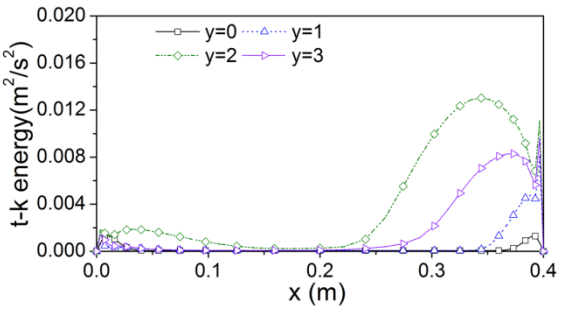

b) H=3m，q_h=200W/m^2，δ=0.4m

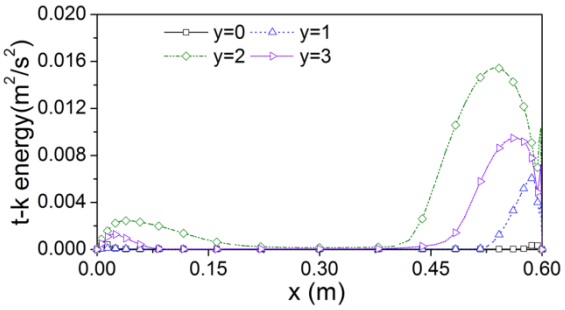

c) H=3m，q_h=200W/m^2，δ=0.6m

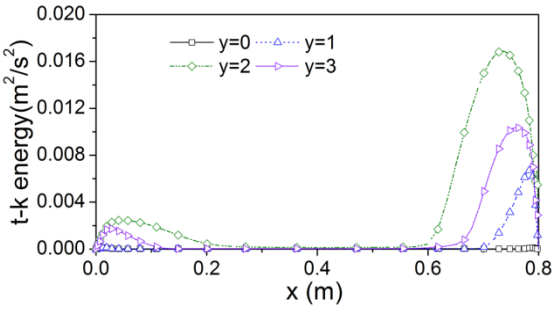

d) H=3m，q_h=200W/m^2，δ=0.8m

Fig. 8 Turbulent kinetic energy distributions at different heights

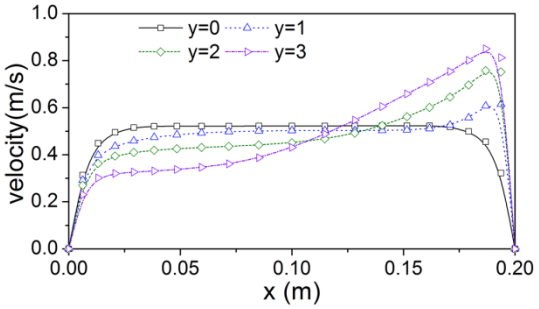

a) H=3m，q_h=200W/m^2，δ=0.2m

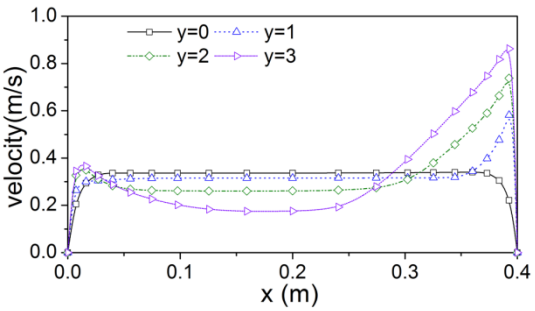

b) H=3m，q_h=200W/m^2，δ=0.4m

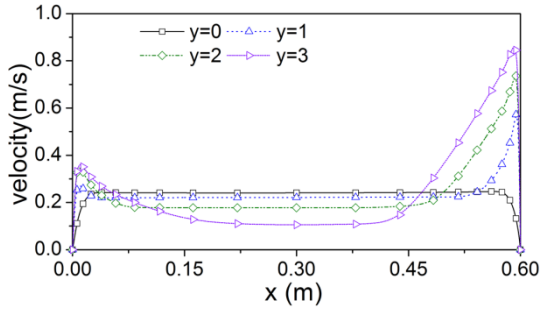

c) H=3m，q_h=200W/m^2，δ=0.6m

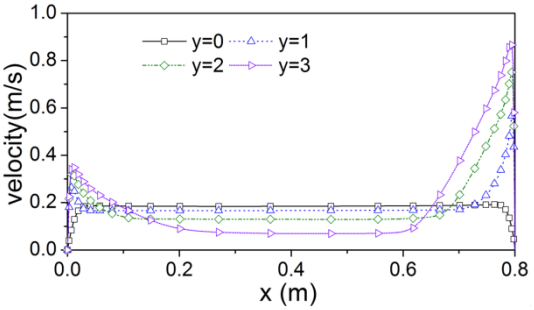

d) H=3m，q_h=200W/m^2，δ=0.8m

Fig.9 Velocity distributions at different heights

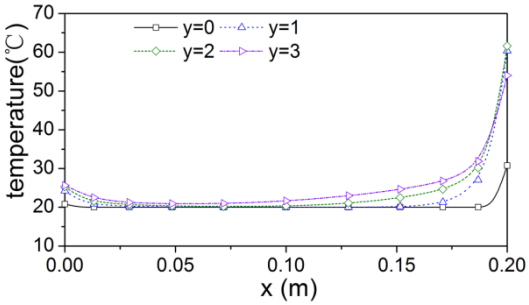

a) H=3m，q_h=200W/m^2，δ=0.2m

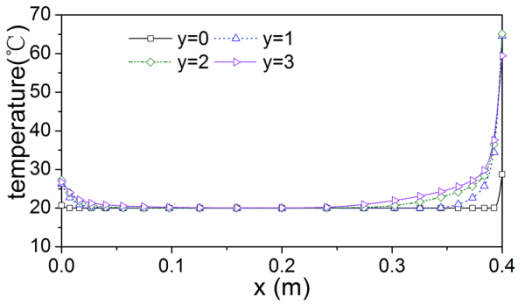

b) H=3m，q_h=200W/m^2，δ=0.4m

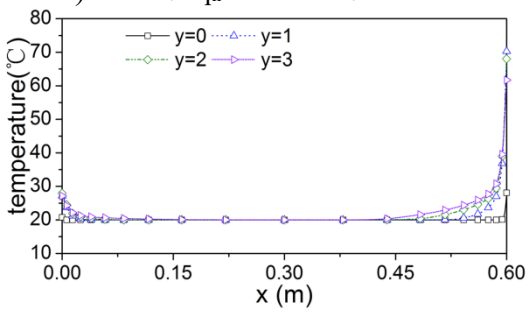

c) H=3m，q_h=200W/m^2，δ=0.6m

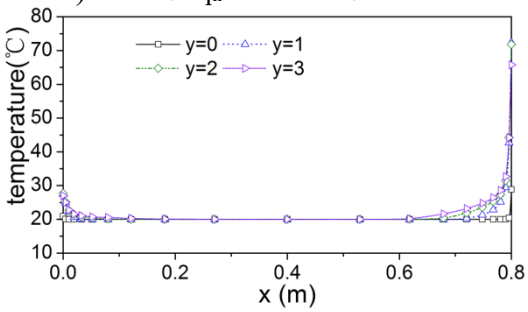

d) H=3m，q_h=200W/m^2，δ=0.8m

Fig. 10 Temperature distributions at different heights

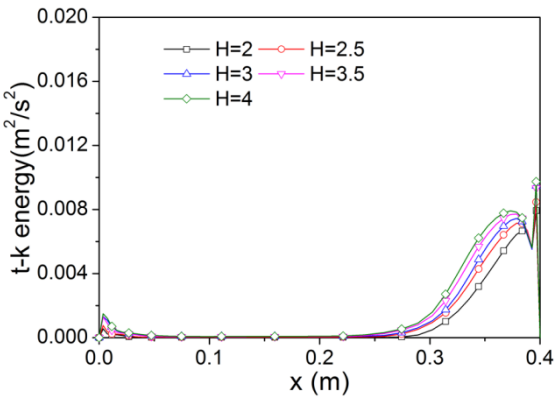

a) y/H=0.5

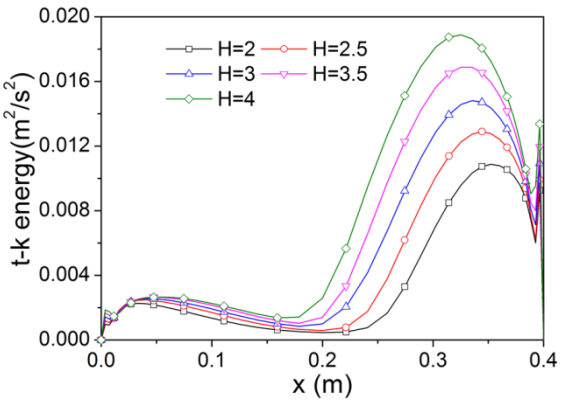

b) y/H=1

Fig.11 Turbulent kinetic energy distributions at y/H=0.5 and y/H=1 in channels with different heights (with heat flux of 200W/m^2 and width of 0.4m)

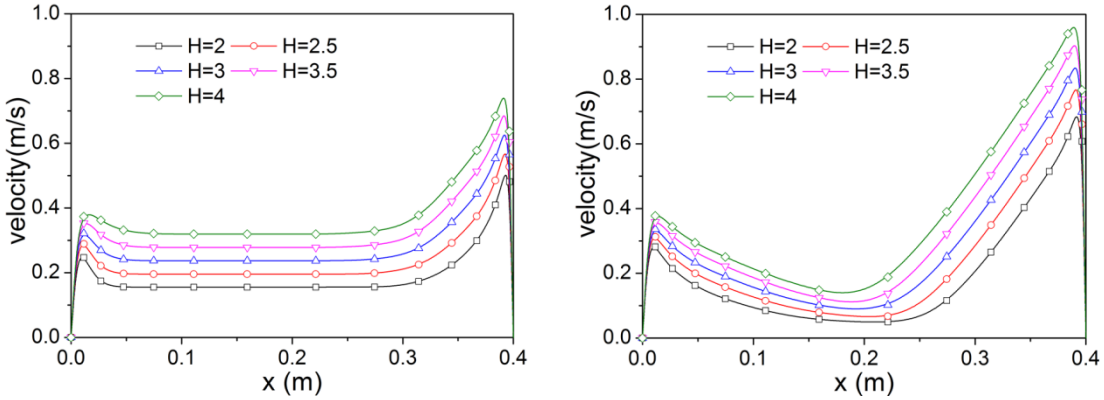

a) y/H=0.5 b) y/H=1

Fig.12 Velocity distributions at y/H=0.5 and y/H=1 in channels with different heights (with heat flux of 200W/m^2 and width of 0.4m)

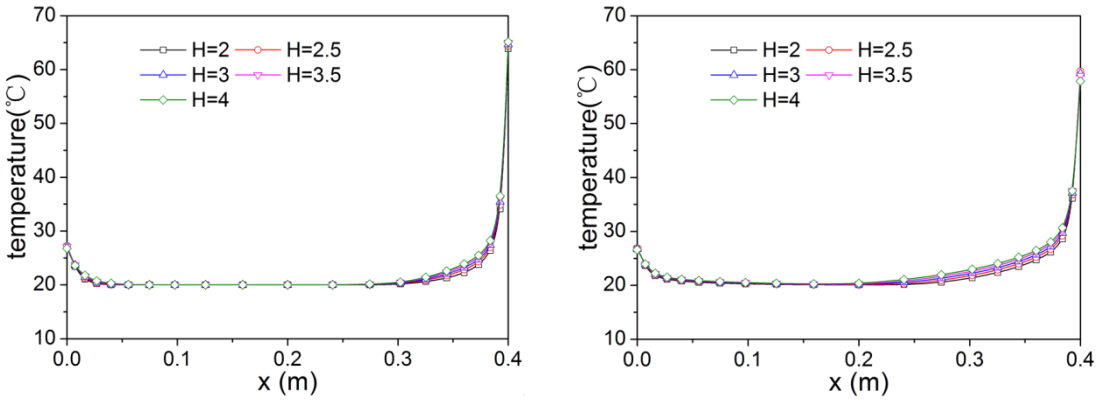

a) y/H=0.5 b) y/H=1

Fig.13 Temperature distributions at y/H=0.5 and y/H=1 in channels with different heights (with heat flux of 200W/m^2 and width of 0.4m)

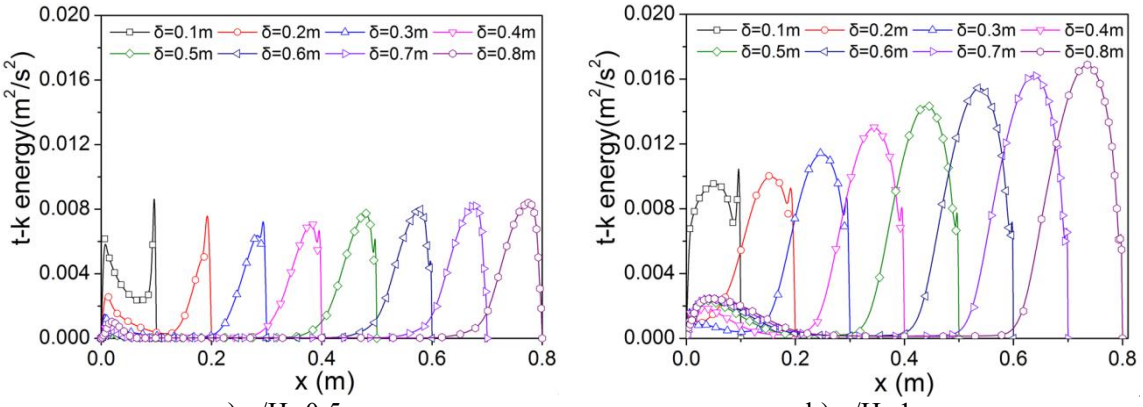

a) y/H=0.5 b) y/H=1

Fig.14 Turbulent kinetic energy distributions at y/H=0.5 and y/H=1 in channels with different widths (with heat flux of 200W/m^2 and height of 3m)

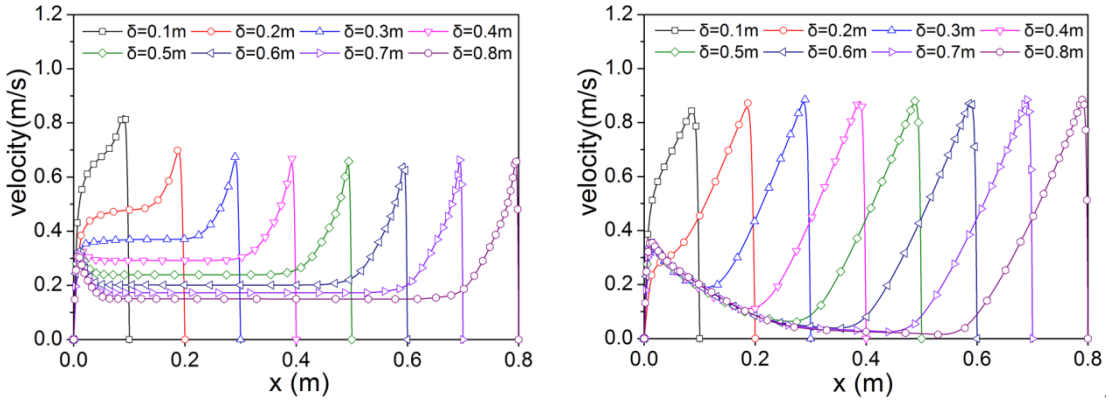

a) y/H=0.5 b) y/H=1

Fig.15 Velocity distributions at y/H=0.5 and y/H=1 in channels with different widths (with heat flux of 200W/m^2 and height of 3m)

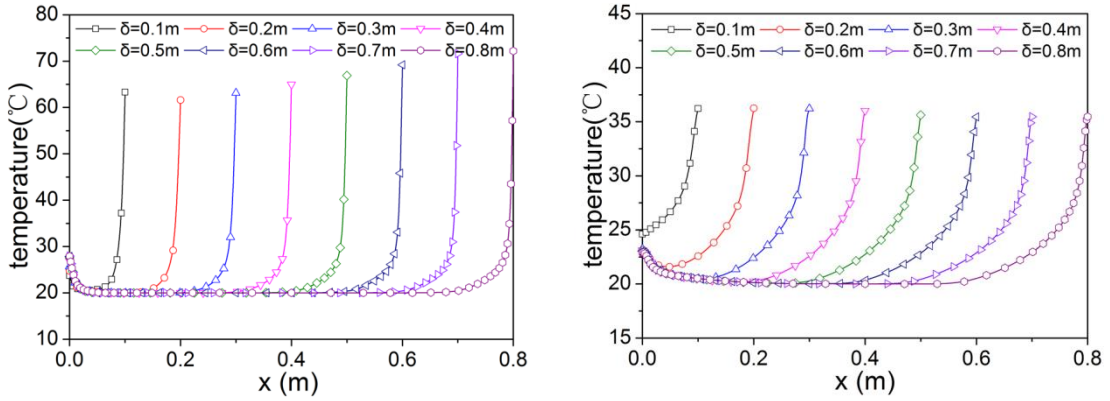

a) y/H=0.5 b) y/H=1

Fig.16 Temperature distributions at y/H=0.5 and y/H=1 in channels with different widths

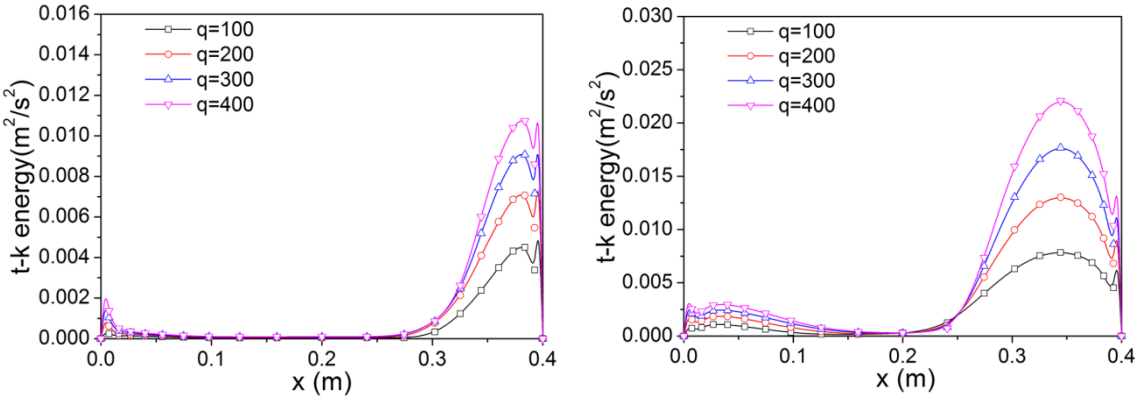

a) y/H=0.5 b) y/H=1

Fig.17 Turbulent kinetic energy distributions at y/H=0.5 and y/H=1 in channels with different heat fluxes

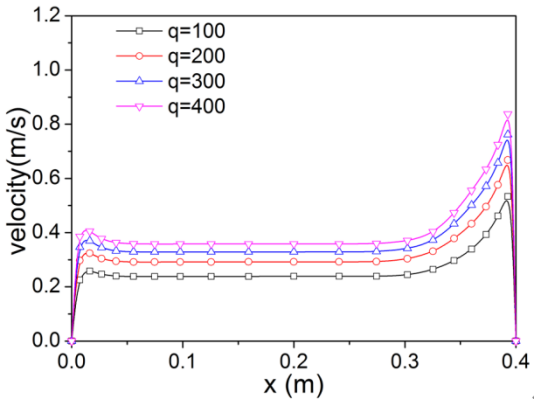

a) y/H=0.5

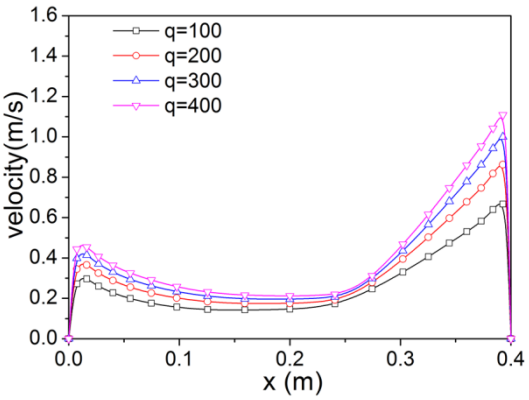

b) y/H=1

Fig.18 Velocity distributions at y/H=0.5 and y/H=1 in channels with different heat fluxes

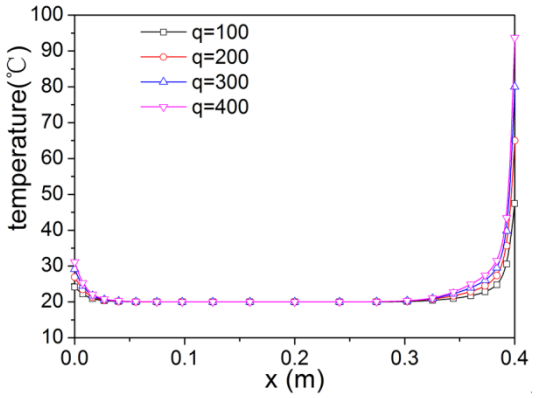

a) y/H=0.5

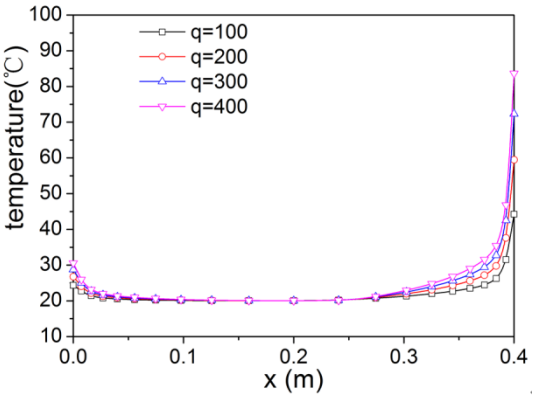

b) y/H=1

Fig.19 Temperature distributions at y/H=0.5 and y/H=1 in channels with different heat fluxes

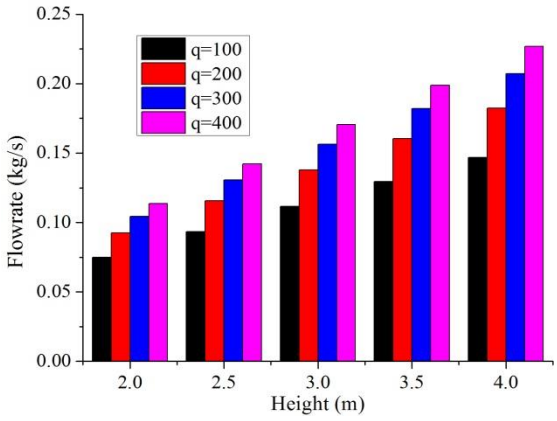

a) air flowrate

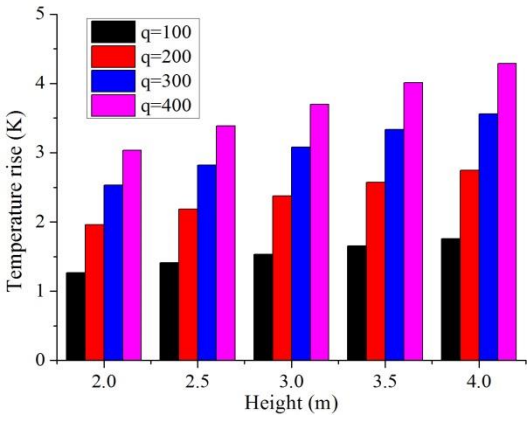

b) temperature rise

Fig.20 Influence of channel height on airflow rate and temperature rise

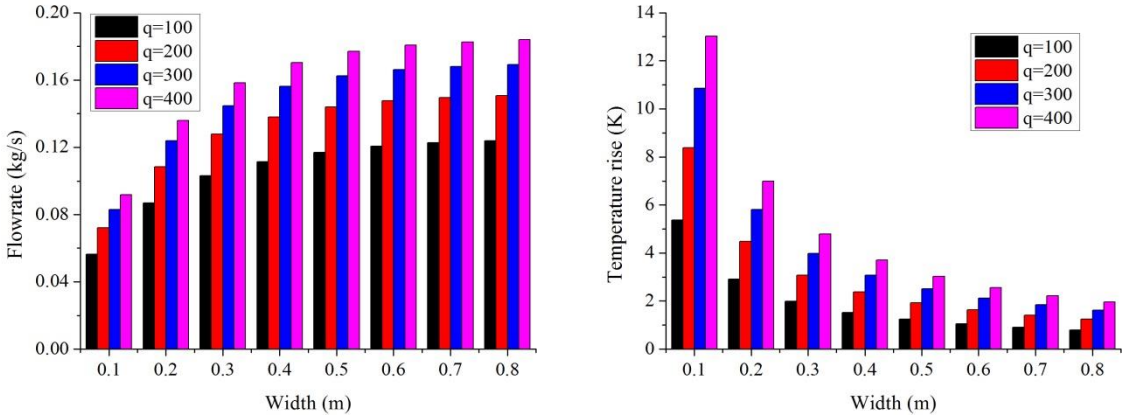

a) air flowrate b) temperature rise

Fig.21 Influence of channel width on airflow rate and temperature rise

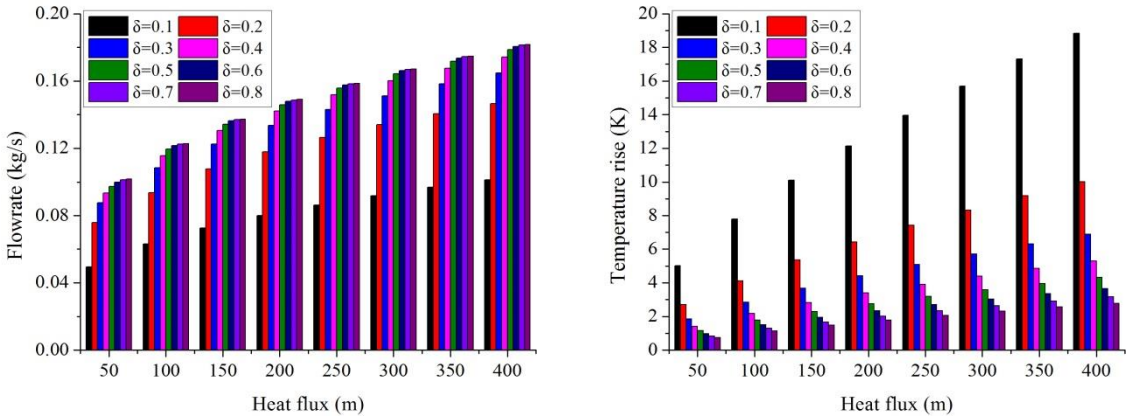

a) air flowrate b) temperature rise

Fig.22 Influence of input heat flux on airflow rate and temperature rise